Available online at www.sciencedirect.com
SCIENCE DIRECT
Journal of Sound and Vibration 296 (2006) 264–276
JOURNAL OF SOUND AND VIBRATION
www.elsevier.com/locate/jsvi

Dispersion curves of fluid filled elastic pipes by standard FE models and eigenpath analysis

Matthias Maess, Nils Wagner, Lothar Gaul*

Institute of Applied and Experimental Mechanics, University of Stuttgart, Pfaffenwaldring 9, D-70550 Stuttgart, Germany

Received 28 February 2005; received in revised form 24 October 2005; accepted 2 March 2006
Available online 6 May 2006

Abstract

This paper presents the application of an alternative waveguide finite element method (WFE) using standard FE-code for the computation of dispersion curves in fluid filled elastic pipes. Only one element is needed in longitudinal direction of the pipe in the FE model, which includes structural–acoustic interaction by a full coupling interface. After rearranging the dynamic stiffness matrix of the segment model in transfer matrix form, a periodicity condition is applied leading to an eigenvalue problem. Here, eigenvectors correspond to wave modes and eigenvalues are a function of the complex wavenumber. From the eigenpairs, phase velocities and group velocities of branches are computed as well as sound power transmission. Instead of solving the eigenvalue problem for each frequency separately, an eigenpath analysis is presented in order to track dispersion curves through the frequency band of interest. The numerical results are compared to results from an analytical model of a thin walled fluid-filled shell. The method allows periodic wave guides with any cross section to be analyzed while employing standard FE discretization.

1. Introduction

The analysis of harmonic wave propagation in piping systems takes a special role in pipe engineering, since continuous conveyance of liquids by pumps and valve actuation generates acoustic sources which may lead to excessive noise levels. In even worse cases, pipe components or attached structural components undergo deterioration. In general, pipes act as a longitudinal waveguide, thus acoustic energy can be transmitted over very large distances. This becomes crucial for low frequency noise in water filled metal pipes, where both structure and fluid barely dissipate energy due to very low viscosities and material damping. The knowledge about sound speed is also important for setting up transfer matrix methods for 1D [1] or 3D [2] pipe components. On the other hand, waveguide properties of pipes are exploited in the context of non-destructive evaluation (NDE), where pipes need to be inspected for cracks or leakage. Harmonic waves, once introduced into pipes, propagate very far. By analyzing times of flight for signals at different receiver points, defect positions or changes of pipe properties can be detected [3]. Both the analysis of unwanted pipe acoustics and

*Corresponding author. Tel.: +49 711 685 6277; fax: +49 711 685 6282.
E-mail address: gaul@mecha.uni-stuttgart.de (L. Gaul).
URL: http://www.mecha.uni-stuttgart.de/Mitarbeiter/Gaul/gaul.htm.

0022-460X/$ - see front matter © 2006 Elsevier Ltd. All rights reserved.
doi:10.1016/j.jsv.2006.03.005

the application for NDE purposes require models for predicting harmonic wave propagation and in particular sound speeds. It was found early that wave propagation in elastic pipes is a strongly dispersive phenomenon [4], resulting in a coexistence of several wave modes with frequency-dependent wavenumbers. As a result, group and phase velocities depend on frequency and wavenumber. A large number of authors analyzed the problem of determining wave dispersion in elastic pipes in recent decades [5–7]. In Ref. [8], a model for an acoustic fluid embedded in a thin elastic cylindrical shell including bending capacities is described. Special spectral finite elements have been developed [9] to determine dispersion in fluid filled elastic pipes by discretized models. Thus, it is possible to obtain waveguide properties for ducts with arbitrary cross sections, where analytical solutions might not be known. Lately, Mace et al. [10,11] introduced a method in order to predict dispersion curves by using standard FE codes. Hereby, dynamic stiffness matrices of segment models are rearranged in transfer matrix form and periodicity conditions are applied in order to recover dispersion curves from an eigenvalue analysis. In the paper at hand, this method is extended to thick walled and thin walled fluid filled elastic pipes, which include a structural–acoustic interface. Furthermore, single dispersion curves may be understood as wavenumber–frequency eigenpath and can be tracked directly as a function of frequency. As a result, the numerical computation of single dispersion curves is accelerated by avoiding the computation of the full or partial spectrum for each frequency of interest.

The main advantage of the presented approach is the computation of dispersion curves for two-field wave guides with arbitrary cross sections while using a standard FE package.

2. Finite element modeling

Approximate discrete solutions of the structural–acoustic field equations [12] are given in terms of the acoustic excess pressure p in the fluid and displacements u in the solid domain, respectively. Applying d'Alembert's principle to the structural field equation and taking the weak form of the wave equation in the fluid leads to a coupled finite element formulation [13] in terms of nodal displacements $\mathbf{u}$ and nodal acoustic pressures $\mathbf{p}$:

$$\underbrace{\begin{bmatrix} \mathbf{M}_s & \mathbf{0} \\ \rho\mathbf{C}^{\mathrm{T}} & \mathbf{M}_f \end{bmatrix}}_{\mathbf{M}} \underbrace{\begin{bmatrix} \ddot{\mathbf{u}} \\ \ddot{\mathbf{p}} \end{bmatrix}}_{\ddot{\mathbf{x}}} + \underbrace{\begin{bmatrix} \mathbf{D}_s & \mathbf{0} \\ \mathbf{0} & \mathbf{D}_f \end{bmatrix}}_{\mathbf{D}} \underbrace{\begin{bmatrix} \dot{\mathbf{u}} \\ \dot{\mathbf{p}} \end{bmatrix}}_{\dot{\mathbf{x}}} + \underbrace{\begin{bmatrix} \mathbf{K}_s & -\mathbf{C} \\ \mathbf{0} & \mathbf{K}_f \end{bmatrix}}_{\mathbf{K}} \underbrace{\begin{bmatrix} \mathbf{u} \\ \mathbf{p} \end{bmatrix}}_{\mathbf{x}} = \begin{bmatrix} \mathbf{f}_s(t) \\ \mathbf{f}_f(t) \end{bmatrix}. \tag{1}$$

Here, mass and stiffness matrices of the acoustic partition in the fluid domain Ω_f are given as

$$\mathbf{M}_f = \int_{\Omega_f} \frac{1}{c^2} \mathbf{R}^{\mathrm{T}}\mathbf{R}\,\mathrm{d}\Omega, \quad \mathbf{K}_f = \int_{\Omega_f} (\mathscr{D}_f\mathbf{R})^{\mathrm{T}}\,\mathscr{D}_f\mathbf{R}\,\mathrm{d}\Omega, \tag{2}$$

where c denotes the free sound speed in the fluid, ρ the mean fluid mass density, $\mathbf{R}$ are interpolation functions in matrix notation and $\mathscr{D}_f$ is a differential operator to build spatial gradients, i.e. $\mathscr{D}_f = \nabla(\cdot)$. Mass and stiffness matrices of the solid partition in domain Ω_s equate as

$$\mathbf{M}_s = \int_{\Omega_s} \rho_s \mathbf{N}^{\mathrm{T}}\mathbf{N}\,\mathrm{d}\Omega, \quad \mathbf{K}_s = \int_{\Omega_s} (\mathscr{D}\mathbf{N})^{\mathrm{T}}\mathscr{E}\mathscr{D}\mathbf{N}\,\mathrm{d}\Omega. \tag{3}$$

The mass density of the solid is denoted by ρ_s, the mechanical stiffness matrix is given by $\mathscr{E}$, whereas $\mathbf{N}$ are interpolation functions and $\mathscr{D}$ denotes differential operators to realize strains from the displacements $\varepsilon = \mathscr{D}\boldsymbol{N}\mathbf{u}$. The coupling matrix $\mathbf{C}$ in Eq. (1) equates as integral over the acoustic fluid–structure interface Γ_i as

$$\mathbf{C} = \int_{\Gamma_i} \mathbf{N}^{\mathrm{T}}\mathbf{n}\mathbf{R}\,\mathrm{d}\Gamma \tag{4}$$

with normal vector $\mathbf{n}$. External nodal structural forces and fluxes are resumed in $\mathbf{f}_s$ and $\mathbf{f}_f$, respectively. Linear damping in the solid and in the fluid enters the system equations (1) as $\mathbf{D}_s$ and $\mathbf{D}_f$, respectively. In this paper, stiffness-proportional damping $\mathbf{D}_s = \beta_s\mathbf{K}_s$ and $\mathbf{D}_f = \beta_f\mathbf{K}_f$ is applied.

3. Computation of dispersion curves by standard FE package

Following the idea of Mace et al. [11], a "segment" model of the wave guide is generated by using standard FE-code [14]. Hereby, a model of a fluid-filled pipe segment as depicted in Fig. 1 is generated by the commercial FE package ANSYS using a structured mesh. Hereby, linear 8-node elements FLUID30 and SOLID45 are employed in the acoustic and in the solid partition, respectively.

All pressure and displacement nodal degrees of freedom are arranged as $\mathbf{x} = [\mathbf{u}^{\mathrm{T}} \ \mathbf{p}^{\mathrm{T}}]^{\mathrm{T}}$ and the forces and fluxes as $\mathbf{f} = [\mathbf{f}_s^{\mathrm{T}} \ \mathbf{f}_f^{\mathrm{T}}]^{\mathrm{T}}$. For time-harmonic system behavior in a waveguide, the dynamic stiffness matrix

$$\mathbf{H}(\omega) = \mathbf{K} + \mathrm{i}\omega\mathbf{D} - \omega^2\mathbf{M} \tag{5}$$

is introduced. Afterwards, the DOFs are partitioned with respect to their positions at the left or right end of the segment model, i.e. $\mathbf{x} = [\mathbf{x}_l^{\mathrm{T}} \ \mathbf{x}_r^{\mathrm{T}}]^{\mathrm{T}}$ and $\mathbf{f} = [\mathbf{f}_l^{\mathrm{T}} \ \mathbf{f}_r^{\mathrm{T}}]^{\mathrm{T}}$. The dynamic stiffness matrix is partitioned accordingly

$$\mathbf{H} = \begin{bmatrix} \mathbf{H}_{ll} & \mathbf{H}_{lr} \\ \mathbf{H}_{rl} & \mathbf{H}_{rr} \end{bmatrix}. \tag{6}$$

It is worth pointing out that the order of "left" DOFs $\mathbf{x}_l$ and "right" DOFs $\mathbf{x}_r$ must be chosen in the same way, such that periodicity conditions for the field variables between the sth and the $s+1$th plane in the segment model fulfil

$$\mathbf{x}_l^{s+1} = \mathbf{x}_r^s \tag{7}$$

for the nodal Dirichlet data and

$$\mathbf{f}_l^{s+1} = -\mathbf{f}_r^s \tag{8}$$

for the nodal Neumann data. Rearrangement leads to the frequency-dependent transfer matrix system

$$\begin{bmatrix} \mathbf{x}_l^{s+1} \\ \mathbf{f}_l^{s+1} \end{bmatrix} = \mathbf{T}(\omega) \begin{bmatrix} \mathbf{x}_l^{s} \\ \mathbf{f}_l^{s} \end{bmatrix} \tag{9}$$

with

$$\mathbf{T}(\omega) = \begin{bmatrix} -\mathbf{H}_{lr}^{-1}\mathbf{H}_{ll} & \mathbf{H}_{lr}^{-1} \\ -\mathbf{H}_{rl} + \mathbf{H}_{rr}\mathbf{H}_{lr}^{-1}\mathbf{H}_{ll} & -\mathbf{H}_{rr}\mathbf{H}_{lr}^{-1} \end{bmatrix}. \tag{10}$$

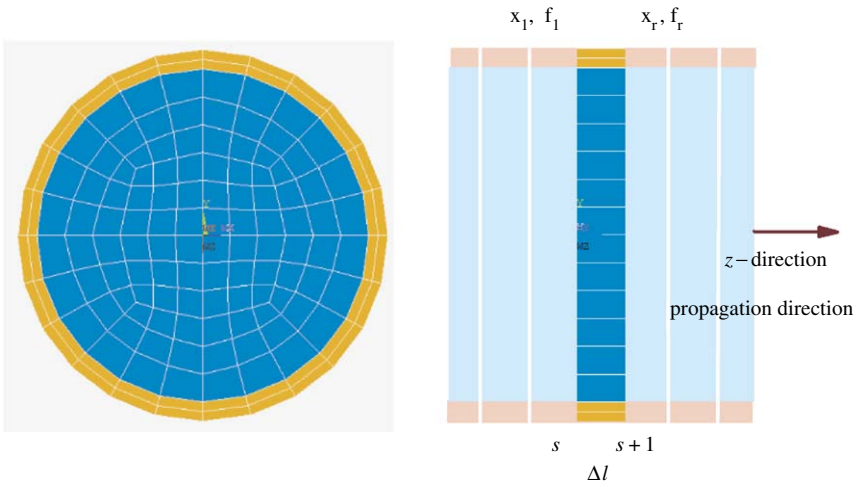

Fig. 1. FE segment model of the thick walled fluid filled pipe by ANSYS.

Assuming harmonic wave propagation in z-direction over the segment length $\Delta\ell$ (Fig. 1) with complex circular wavenumber κ

$$\begin{aligned}\mathbf{x}_r &= \mathrm{e}^{\kappa\Delta\ell}\mathbf{x}_l,\\ \mathbf{f}_r &= \mathrm{e}^{\kappa\Delta\ell}\mathbf{f}_l,\end{aligned} \tag{11}$$

leads to the eigenvalue problem

$$\mathbf{T}(\omega)\begin{bmatrix}\hat{\mathbf{x}}_l(\omega)\\ \hat{\mathbf{f}}_l(\omega)\end{bmatrix} = \mathrm{e}^{\kappa\Delta\ell}\begin{bmatrix}\hat{\mathbf{x}}_l(\omega)\\ \hat{\mathbf{f}}_l(\omega)\end{bmatrix} = \lambda\begin{bmatrix}\hat{\mathbf{x}}_l(\omega)\\ \hat{\mathbf{f}}_l(\omega)\end{bmatrix}. \tag{12}$$

As an alternative, the generalized eigenvalue problem

$$\begin{bmatrix}\mathbf{H}_{ll} & -\mathbf{I}\\ \mathbf{H}_{rl} & \mathbf{0}\end{bmatrix}\begin{bmatrix}\hat{\mathbf{x}}_l\\ \hat{\mathbf{f}}_l\end{bmatrix} = \lambda\begin{bmatrix}-\mathbf{H}_{lr} & \mathbf{0}\\ -\mathbf{H}_{rr} & \mathbf{I}\end{bmatrix}\begin{bmatrix}\hat{\mathbf{x}}_l\\ \hat{\mathbf{f}}_l\end{bmatrix} \tag{13}$$

may be considered. The physical complex wavenumber κ is retrieved from the eigenvalues by

$$\kappa = \frac{\ln(\lambda)}{\Delta\ell}. \tag{14}$$

For a fixed frequency ω, the number of numerically computed solutions of κ is as many as the dimension of $\mathbf{T}$. Also, the eigenvalues occur in pairs of λ_j and $1/\lambda_j$ [11] representing left-propagating and right-propagating wave modes. However, only a very limited number of eigenvalues represent physical solutions of interest. First, right-propagating wave modes with $|\lambda|>1$ increase their amplitude according to Eq. (11) while propagating, and are considered non-physical. Therefore, $|\lambda|\leqslant 1$ is a necessary condition. This becomes evident from the fact that λ can be written in the complex plane as

$$\lambda = |\lambda|\ \mathrm{e}^{\mathrm{i}(\phi+2\pi m)}, \quad m = 0, 1, 2, 3\ldots \tag{15}$$

and

$$\ln(\lambda) = \ln(|\lambda|) + \mathrm{i}(\phi + 2\pi m). \tag{16}$$

The modification of wave amplitudes is given by the real part of the complex wavenumber. Wave modes are exponentially decaying if $|\lambda|<1$ while maintaining their amplitude only if $|\lambda| = 1$. If wave modes have a purely negative real part of the wavenumber, they represent evanescent waves and are excluded from the further analysis. Fig. 2 displays the spectrum only in the vicinity of the unit circle. Eigenvalues may also be excluded for engineering reasons if $|\lambda|\ll 1$, such that they are oscillatory but decaying very quickly. Furthermore, the imaginary part of the wavenumber is represented by negative angles ϕ in the complex plane, if waves are right-propagating. Note that the logarithm is not uniquely defined in the complex plane, since m in Eq. (15) does not necessarily equal zero. However, the analysis in Section 3.1 reveals that physical relevant wavenumbers cannot be characterized by $m>0$. The area of interest is therefore restricted to eigenvalues on or within the unit circle with radius $r = |\lambda| = 1$ for negative imaginary values. Note that positive imaginary values in the upper half of the complex plane denote left-propagating waves, which contain redundant information and are therefore excluded from further analysis. If dispersion curves are tracked while increasing frequency ω, one finds that eigenvalues belonging to (undamped) propagating wave modes move on the unit circle in clockwise direction (in negative ϕ-direction), if wavenumbers increase as well.

The method is applied for a water-filled brass pipe as found in cooling systems of ships, here denoted as thick walled pipe ($h/a = 0.11$). Dimensions and material properties of the shell are listed in Table 1 and fluid properties are given by $c = 1481\,\mathrm{m/s}$ and $\rho = 1000\,\mathrm{kg/m^3}$.

The segment model has a number of 674 DOFs, thereof 432 structural DOFs and 242 pressure DOFs. Frequencies are normalized with respect to the ring frequency $\Omega = \omega/\omega_r$, which equates as $\omega_r = c_{shell}/a$. The eigenvalues λ are plotted for $\Omega = 1.49$ and $\Delta\ell = 5\,\mathrm{mm}$ in the complex plane as depicted in Fig. 2. First, damping is excluded, thus $\mathbf{D} = \mathbf{0}$ ($\beta_s = \beta_f = 0$, marker $+\,+$), and eigenvalues representing non-decaying propagating wave modes are on the unit circle. If damping is applied ($\beta_s = \beta_f = 1.5\times 10^{-6}$, marker $o\ o$, and

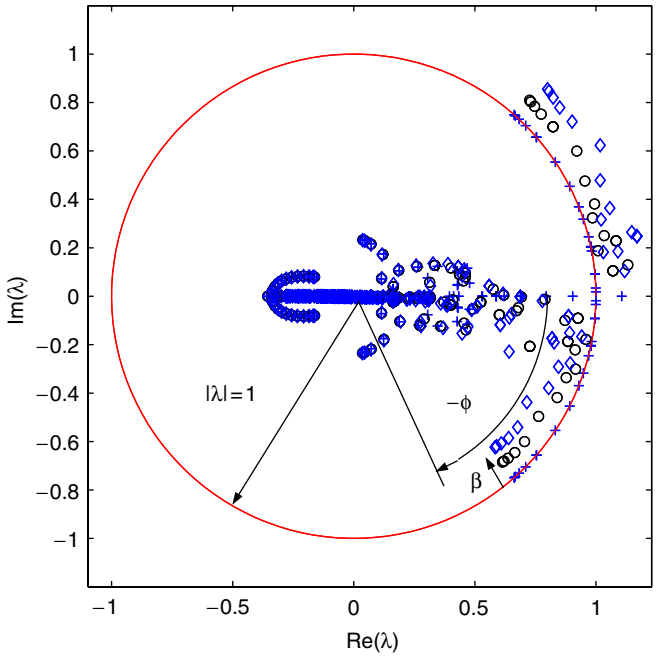

Fig. 2. Eigenvalues at $\Omega = 1.49$ for various damping values $\beta_s = \beta_f = 0(+), \beta_s = \beta_f = 1.5 \times 10^{-6}(o), \beta_s = \beta_f = 3 \times 10^{-6}$ ($\diamond$).

Table 1
Properties of the thick walled and of the thin walled brass pipe

	Mean radius a (m)	Thickness h (m)	Young's modulus (N/m^2)	Density ρ_s (kg/m^3)
Thick	0.036	0.004	1.35×10^{11}	8900
Thin	0.036	0.002	1.35×10^{11}	8900

$\beta_s = \beta_f = 3 \times 10^{-6}$, marker $\diamond$ $\diamond$), eigenvalues λ decrease their absolute value, thus the corresponding wave mode amplitudes decay exponentially.

In order to obtain the complete dispersion diagram, the method according to Mace et al. [11] is applied for all frequencies of interest. In the following analysis, damping is neglected by setting again $\mathbf{D} = \mathbf{0}$. Propagating wave modes with a purely imaginary wavenumber are depicted in the dispersion diagram in Fig. 3. Note that imaginary parts of the wavenumber denoting the propagating part of the wavenumber are made non-dimensional by multiplication with shell mean radius a. Solid-type waves are marked by solid lines. Branch 1 is the extensional shell mode for low frequencies, whereas branch 3 corresponds to the torsional shell mode, which barely couples to the fluid and turns out to be almost non-dispersive. Branch 2 is an axis-symmetric shell mode cutting on near the ring frequency of the pipe near $\Omega = 1$. Dashed lines denote shell beam modes, whereas fluid-type wave modes are depicted as dotted lines. Branch 4 is the fluid-type mode corresponding to a plane wave in a rigid duct. A complete discussion of wave modes in fluid filled shells is given in Ref. [8]. Wave modes are conveniently visualized by displaying wall deformations and the coupled acoustic pressure field as contour plot contained in eigenvectors $\hat{\mathbf{x}}_l$ from Eq. (12). Fig. 4 shows wave modes for $\Omega = 0.765$ of the $n = 0$-bending mode (left, marker '+' in Fig. 3) and of the $n = 4$-bending mode (right, marker 'o' in Fig. 3).

3.1. Influence of mesh size on wavenumbers

The use of discretized models for the determination of complex wavenumbers is encompassed by discretization errors if results are compared to exact solutions of continuous systems. Using approximations

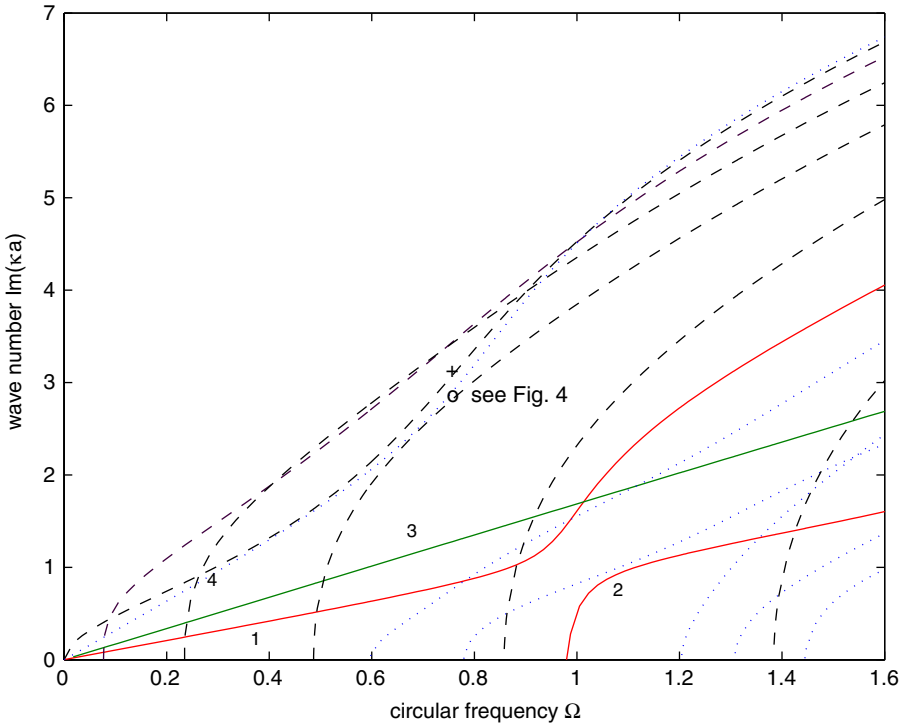

Fig. 3. Dispersion diagram of wave modes in a water-filled thick walled brass pipe ($h/a = 0.11$) with segment length $\Delta\ell = 5\,\text{mm}$. Fluid-type modes (···), extensional/torsional shell modes (—) and beam-type modes (- - -) are distinguished.

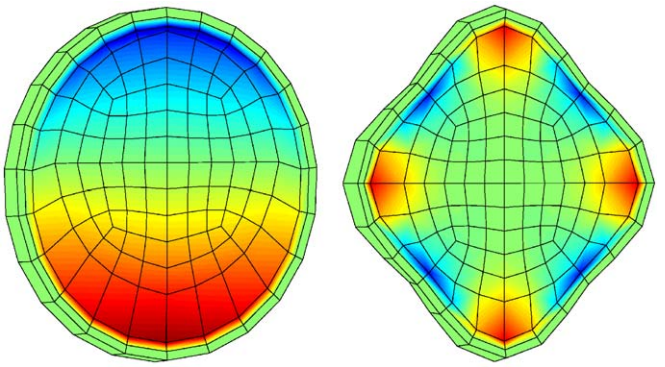

Fig. 4. Wave forms for $\Omega = 0.765$ of the $n = 0$-bending mode (left,'+' in Fig. 3) and of the $n = 4$-bending mode (right, 'o' in Fig. 3): Deformation of the shell and pressure field in the fluid.

for the field variable results in most cases in increased eigenfrequencies as shown by Rayleigh's quotient in case of the first vibrating mode. Stiffening does also affect increased sound speeds of propagating wave modes. For comparison, the results by postprocessed FE models of a thin walled pipe ($h/a = 0.056$, Table 1) are compared to numerical results by an analytical model using Flügge's shell theory [2] for thin walled pipes. The agreement of dispersion curves is depicted in Fig. 5, where $n = 0$-branches, i.e. axis-symmetric wave modes, of the analytical approach ($\times\,\times$) are compared to wave modes obtained by the FE-model. First, a model with segment length $\Delta\ell = 10\,\text{mm}$ (– –) is employed. Slight deviations from the analytical approach for the cut-on mode near the ring frequency (branch 2) and for the extensional shell mode (branch 1) occur. They are considered to result from defects of Flügge's thin walled shell equations and from the discretization, since no curvilinear elements are used in circumferential shell direction. Focusing on the fluid-mode (branch 4), it is

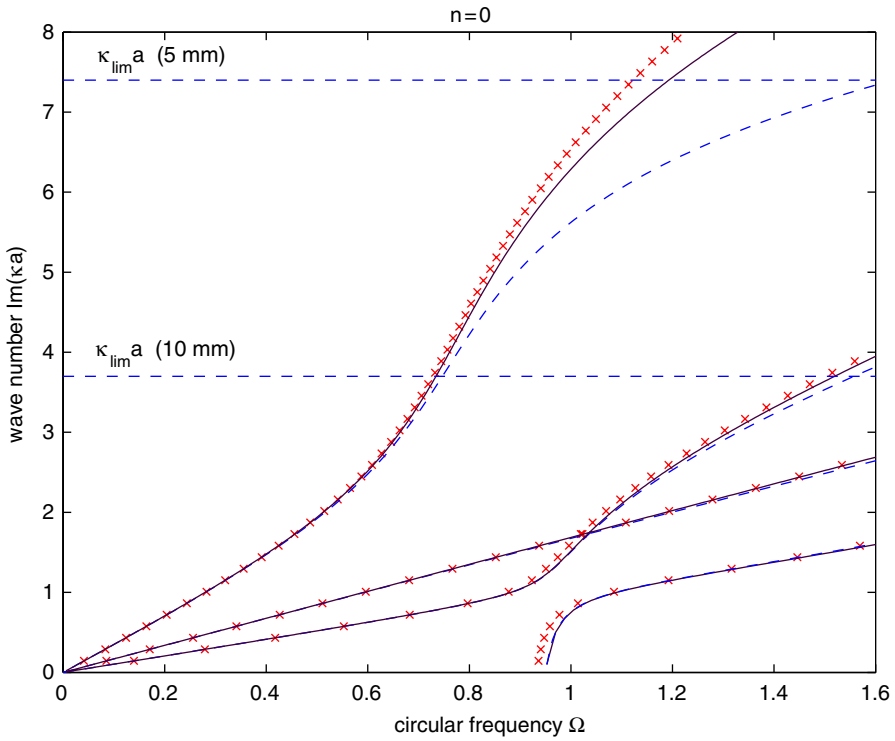

Fig. 5. Underestimation of wave numbers due to finite element approximation for axis-symmetric $n = 0$-modes in a thin walled brass pipe ($h/a = 0.056$): Analytical solution ($\times\,\times$), longitudinal mesh size $\Delta\ell = 5$ mm (—), longitudinal mesh size $\Delta\ell = 10$ mm (– –).

evident that a systematic error occurs above wavenumbers $\kappa a > 4$. If one applies the rule of thumb in acoustics, i.e. n_e linear elements should be used at least per wavelength (minimum $n_e = 6$), one equates theoretically the non-dimensional wavenumber $\kappa_{\lim} a = 3.7$, depicted as horizontal dashed line. If the segment length is reduced to $\Delta\ell = 5$ mm encompassed by mesh refinement (branches —), the confidelity range is further increased (theoretically $\kappa_{\lim} a = 7.4$ for 6 linear elements). In the computed range, the deviations are reduced for branch 4. Similar results are deduced by analyzing errors of asymmetric $n = 1$-modes in Fig. 6. Deviations are deduced for the Bernoulli beam-type bending mode (B). As a general result, one finds that errors due to coarse discretization follow the standard rule of thumb from finite element method. As a consequence, mesh refinement improves the accuracy of the results and an h-adaptive strategy may serve as indicator to check convergence of the approximate solution.

Formulating the rule of thumb with Eq. (15) results in the inequality

$$\frac{2\pi}{n_e \Delta\ell} \geqslant |\Im(\kappa)| = \frac{\ln(\lambda)}{\Delta\ell} = \frac{|\phi + 2\pi m|}{\Delta\ell}. \tag{17}$$

Hence, the condition $|\phi + 2\pi m| \leqslant 2\pi/n_e$ is imposed. Recalling that only negative values are of relevance for ϕ in the complex plane (compare Fig. 2) and that $m = 0$ by considering the results in the dispersion diagram, one obtains for $n_e = 6$ the value $-1.04 \leqslant \phi \leqslant 0$. It should be mentioned that in general, right-propagating waves may also have a negative group velocity [10], or in other words, left-propagating wave modes transfer energy to the right. In this case, the possible segment for the phase angle ϕ for wave modes of interest in Eq. (17) has to be extended to positive values. However, this case does not occur in any of the presented results.

3.2. Numerical treatment of the eigenvalue problem

The first remark addresses to the inversion of submatrix $\mathbf{H}_{lr}$. Eigenanalysis of corresponding mass and stiffness partitions $\mathbf{M}_{lr}$ and $\mathbf{K}_{lr}$ show that eigenvalues occur in the frequency range of interest. This means that

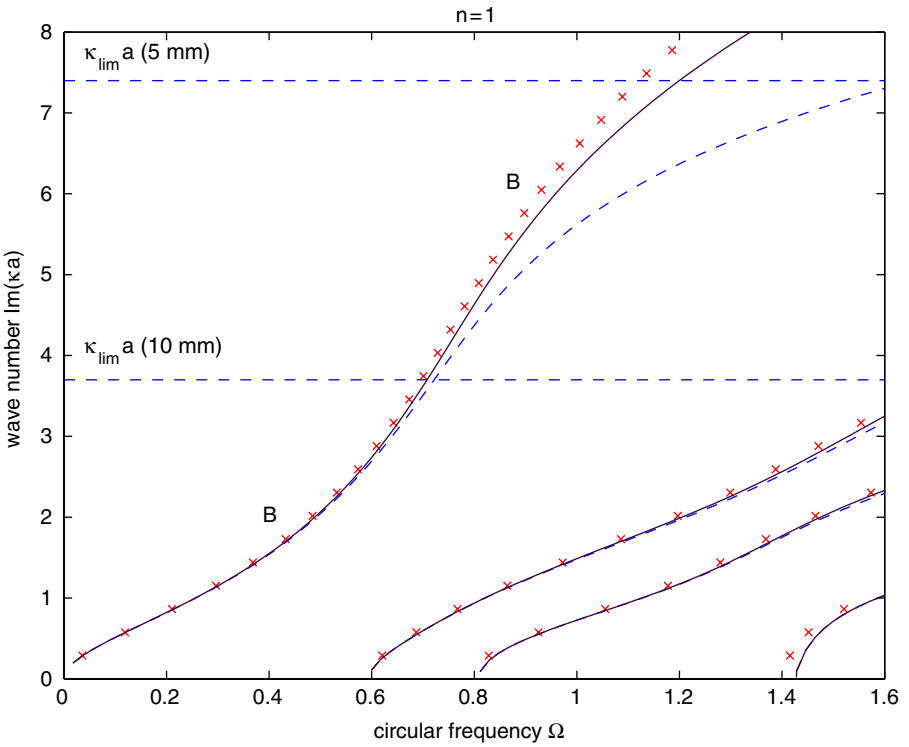

Fig. 6. Underestimation of wavenumbers due to finite element approximation for asymmetric $n = 1$-modes in a thin walled brass pipe ($h/a = 0.056$): Analytical solution ($\times\ \times$), longitudinal mesh size $\Delta\ell = 5\,\text{mm}$ (—), longitudinal mesh size $\Delta\ell = 10\,\text{mm}$ (– –).

at these eigenfrequencies, $\mathbf{H}_{lr}$ cannot be inverted. However, the methodology gives results for frequencies ω that are very close to these eigenfrequencies. From an engineering point of view, the method can be applied, since the chance of hitting on the singularity of $\mathbf{H}_{lr}$ can be avoided.

The efficient solution of the eigenvalue problem according to Eq. (9) or (13) involves numerical difficulties. Firstly, the system matrices are ill-conditioned and require preconditioning [15]. This problem refers to both the generalized and the special eigenvalue problem. Secondly, wave modes occur twice for axis-symmetric waveguides, such that multiple eigenvalues occur in the spectrum. A crude way to solve the eigenvalue problem is therefore to use an eigensolver based on QR algorithm [16]. Only wave modes of interest, i.e. propagating wave modes with an imaginary wave number are further considered. This method works very accurately even for multiple eigenvalues and eigenvectors, but requires large computing times. It turns out that solving the generalized eigenvalue problem increases computing times due to conditioning problems, even though the submatrix $\mathbf{H}_{lr}$ needs not to be inverted.

4. Computation of phase velocities and group velocities

From the dispersion curves, the phase velocities are deduced easily by the relation

$$c_p = \frac{\omega}{\kappa}. \tag{18}$$

On the other hand, one is particularly interested in group velocities describing the speed by which energy is transmitted in wave packages. Group velocities are defined from the dispersion curves [17] as

$$c_g = \frac{\partial\omega}{\partial\kappa}. \tag{19}$$

This equation requires a numerical derivation of the wave modes from discrete pairs (ω, κ) resulting in relatively large errors. For this reason, it is more convenient to express the group velocity as velocity at which

energy propagates, i.e. the ratio of transmitted power P and energy density $\bar{E}$ in the waveguide

$$c_g = \frac{P}{\bar{E}} = \frac{P_f + P_s}{\bar{T}_s + \bar{T}_f + \bar{U}_s + \bar{U}_f}. \tag{20}$$

Eq. (20) splits all terms according to their contribution to solid domain or fluid domain. For the structural–acoustic problem, energy densities are computed by means of system matrices and wave modes, i.e. the partitions of the eigenvectors in Eq. (12). The kinetic energy T_s and the potential energy U_s in a linear–elastic solid segment are given as

$$T_s = \int_{\Omega_s} \frac{1}{2}\rho_s \tilde{v}^2 \,\mathrm{d}\Omega, \quad U_s = \int_{\Omega_s} \frac{1}{2}\Re(\tilde{\sigma} : \tilde{\varepsilon}^{\mathrm{H}}) \,\mathrm{d}\,\Omega \tag{21}$$

in terms of particle velocities v, linear strain tensor ε and Cauchy stress tensor σ respectively. Subscript $(\cdot)^{\mathrm{H}}$ denotes complex conjugate transposed values. The tilde denotes root mean square values to take into account the effective time-averaged energy density in the acoustic field for harmonic wave propagation as compared to the amplitude values. In discrete FE-representation, energy densities in a pipe segment of length $\Delta\ell$ equate in agreement with Eq. (3) as

$$\bar{T}_s = \frac{1}{4\Delta\ell}\omega^2 \hat{\mathbf{u}}^{\mathrm{H}} \mathbf{M}_s \hat{\mathbf{u}}, \quad \bar{U}_s = \frac{1}{4\Delta\ell}\hat{\mathbf{u}}^{\mathrm{H}} \mathbf{K}_s \hat{\mathbf{u}}. \tag{22}$$

Note that time-averaging leads to the four in the denominator, since $\tilde{\mathbf{u}} = \hat{\mathbf{u}}/\sqrt{2}$. In the acoustic domain, kinetic and potential energy are expressed as [18]

$$T_f = \int_{\Omega_f} \frac{1}{2}\rho \tilde{v}^2 \,\mathrm{d}\Omega, \quad U_f = \int_{\Omega_f} \frac{1}{2\rho c^2}\tilde{p}^2 \,\mathrm{d}\Omega. \tag{23}$$

Carrying out these expressions rigorously by employing definitions for the acoustic mass and stiffness matrices from Eq. (2) and by applying Euler's equation in the frequency domain

$$\mathrm{i}\omega\rho\hat{\mathbf{v}} = -\nabla\hat{\mathbf{p}}, \tag{24}$$

energy densities in the acoustic fluid equate from discrete wave modes as

$$\bar{T}_f = \frac{1}{4\Delta\ell\rho\omega^2}\hat{\mathbf{p}}^{\mathrm{H}} \mathbf{K}_f \hat{\mathbf{p}}, \quad \bar{U}_f = \frac{1}{4\Delta\ell\rho}\hat{\mathbf{p}}^{\mathrm{H}} \mathbf{M}_f \hat{\mathbf{p}}. \tag{25}$$

It is worth mentioning that the *stiffness* matrix enters the *kinetic* energy density, while the *mass* matrix governs the *elastic* energy density in the pipe segment. This is in agreement with the observation that the so-called mass matrix $\mathbf{M}_f$ does not represent generalized mass in a physical sense [19].

Time-averaged power flows P over pipe cross sections Γ_s and Γ_f, see Fig. 7, are given as

$$P_s = \int_{\Gamma_s} \tilde{\sigma}\tilde{\mathbf{v}} \,\mathrm{d}\Gamma, \quad P_f = \int_{\Gamma_f} \tilde{p}\tilde{\mathbf{v}} \,\mathrm{d}\Gamma. \tag{26}$$

In terms of discrete results for wave modes, power flows become in the frequency domain

$$P_s = \tfrac{1}{2}\omega\Im(\hat{\mathbf{f}}_s^{\mathrm{H}}\hat{\mathbf{u}}) \tag{27}$$

for the cross section of the solid domain and

$$P_f = \frac{1}{2\rho\omega}\Im(\hat{\mathbf{q}}^{\mathrm{H}}\hat{\mathbf{p}}) \tag{28}$$

for the cross section of the fluid domain, respectively. Despite the use of some algebra in Eqs. (20)–(28), the group velocities are computed accurately by Eq. (20) without large numerical effort. Group velocities for all propagating wave modes in the thick walled brass pipe are depicted in Fig. 8.

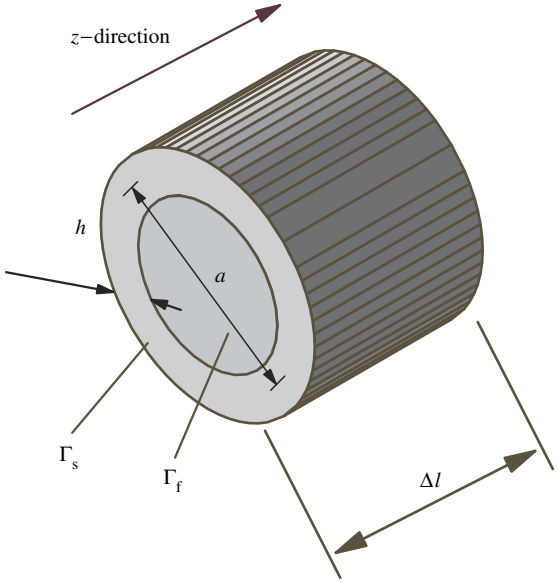

Fig. 7. Geometric properties of the segment model.

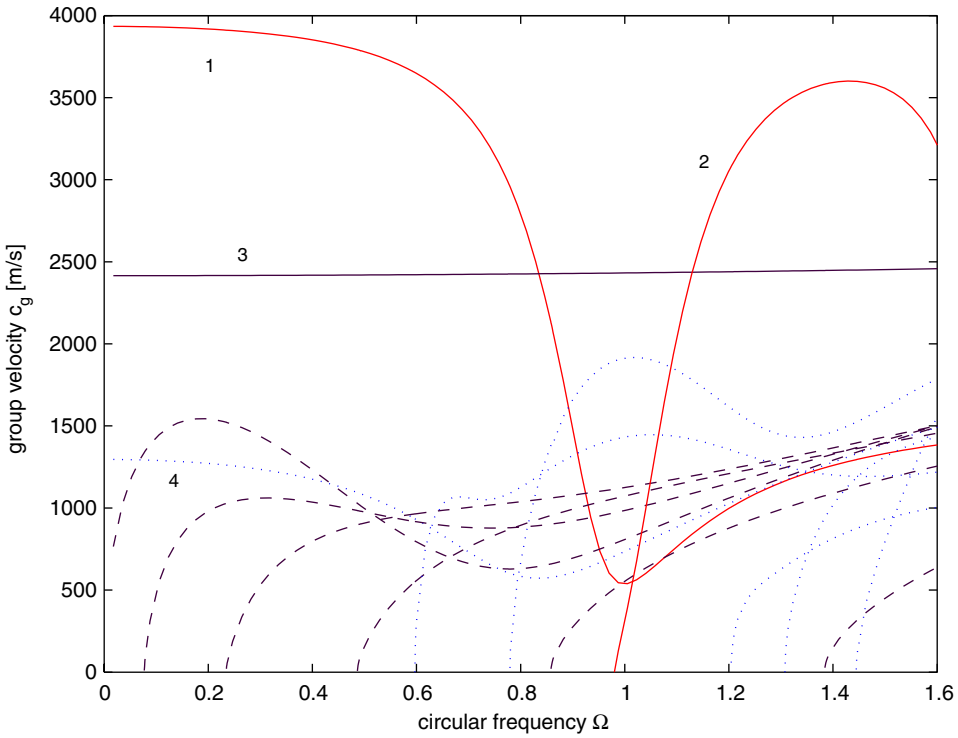

Fig. 8. Group velocities in the water-filled brass pipe. Fluid-type modes (···), extensional/torsional shell modes (—) and beam-type modes (- - -) are distinguished.

5. Eigenpath analysis

In practical applications, one might be interested in tracking only single dispersion curves through the dispersion diagram such as in the case of parameter variations. On the other hand, it is evident from Eqs. (12)

and (13) that eigenvalues λ and eigenvectors $\hat{\mathbf{e}} = [\hat{\mathbf{x}}^{\mathrm{T}}\hat{\mathbf{f}}^{\mathrm{T}}]^{\mathrm{T}}$ are functions of frequency ω. Therefore, wave modes are computed by eigenvalue analysis for a given frequency ω_j. However, frequency can be understood as varying parameter in the system of equations. Instead of solving the time-consuming full or partial eigenvalue problem again for other frequencies of interest $\omega_{j+1} = \omega_j + \Delta\omega$, one is interested in the change of $\hat{\mathbf{e}}_j(\omega_j)$ and $\lambda_j(\omega_j)$ to conclude on $\hat{\mathbf{e}}_{j+1}(\omega_{j+1})$ and $\lambda_{j+1}(\omega_{j+1})$ at this new frequency. This problem is referred to as an eigenpath analysis [20], where branches mark frequency-dependent eigenpaths. It is therefore intended to generate the dispersion curves in Fig. 3 by an eigenpath analysis. An initial solution for one ω_j is needed to start the algorithm. In case of the fluid filled pipes, it is recommendable to start with the highest ω of interest, and to choose the increments $\Delta\omega < 0$, thus following dispersion curves from right to left. Hereby, the problem of missing cut-on modes as seen in Fig. 3 is circumvented as compared to a left-right scheme. Two solution steps, namely predictor and corrector step, are performed for this analysis.

A *predictor step* is applied first. For convenient notation, eigenvectors are written as $\hat{\mathbf{e}} = [\hat{\mathbf{x}}^{\mathrm{T}}\ \ \hat{\mathbf{f}}^{\mathrm{T}}]^{\mathrm{T}}$. Eigenvectors and eigenvalues are expanded as Taylor series

$$\hat{\mathbf{e}}_{j+1} = \hat{\mathbf{e}}_j + \left.\frac{\partial\hat{\mathbf{e}}}{\partial\omega}\right|_{\omega=\omega_j}\Delta\omega + \mathcal{O}(\Delta\omega^2),$$
$$\lambda_{j+1} = \lambda_j + \left.\frac{\partial\lambda}{\partial\omega}\right|_{\omega=\omega_j}\Delta\omega + \mathcal{O}(\Delta\omega^2). \tag{29}$$

By inserting the linear terms of this series in the eigenvalue problem (9) and by using the normalization $\hat{\mathbf{e}}_j^{\mathrm{H}}\hat{\mathbf{e}}_{j+1} = 1$, one obtains the system of equation

$$\begin{bmatrix} -(\mathbf{T} - \lambda_j\mathbf{I}) & \hat{\mathbf{e}}_j \\ \mathbf{e}_j^{\mathrm{H}} & 0 \end{bmatrix}\begin{bmatrix} \hat{\mathbf{e}}' \\ \lambda' \end{bmatrix} = \begin{bmatrix} \mathbf{T}'\hat{\mathbf{e}}_j \\ 0 \end{bmatrix}. \tag{30}$$

The operator $(\cdot)'$ denotes partial derivative with respect to ω. The partial derivative $\partial\mathbf{T}/\partial\omega = \mathbf{T}'$ equates as

$$\mathbf{T}' = \begin{bmatrix} -(\mathbf{H}_{lr}^{-1})'\mathbf{H}_{ll} - \mathbf{H}_{lr}^{-1}\mathbf{H}_{ll} & (\mathbf{H}_{lr}^{-1})' \\ -(\mathbf{H}_{lr}^{-1})' + \mathbf{H}_{rr}'\mathbf{H}_{lr}^{-1}\mathbf{H}_{ll} + \mathbf{H}_{rr}\mathbf{A} & -\mathbf{H}_{rr}'\mathbf{H}_{lr}^{-1} - \mathbf{H}_{rr}(\mathbf{H}_{lr}^{-1})' \end{bmatrix} \tag{31}$$

with abbreviation $\mathbf{A} = [(\mathbf{H}_{lr}^{-1})'\mathbf{H}_{ll} + \mathbf{H}_{lr}^{-1}\mathbf{H}_{ll}']$. The partial derivatives of the inverses are computed by using the relation

$$(\mathbf{H}_{lr}\mathbf{H}_{lr}^{-1})' = \mathbf{H}_{lr}'\mathbf{H}_{lr}^{-1} + \mathbf{H}_{lr}(\mathbf{H}_{lr}^{-1})' = \mathbf{0}, \tag{32}$$

thus rendering

$$\begin{aligned}(\mathbf{H}_{lr}^{-1})' &= \frac{\partial}{\partial\omega}((\mathbf{K}_{lr} + \mathrm{i}\omega\mathbf{C}_{lr} - \omega^2\mathbf{M}_{lr})^{-1}) \\ &= (\mathbf{K}_{lr} + \mathrm{i}\omega\mathbf{C}_{lr} - \omega^2\mathbf{M})^{-1}(-\mathrm{i}\mathbf{C}_{lr} + 2\omega\mathbf{M}_{lr})(\mathbf{K}_{lr} + \mathrm{i}\omega\mathbf{C}_{lr} - \omega^2\mathbf{M}_{lr})^{-1} \\ &= \mathbf{H}_{lr}^{-1}(-\mathrm{i}\mathbf{C}_{lr} + 2\omega\mathbf{M}_{lr})\mathbf{H}_{lr}^{-1}.\end{aligned} \tag{33}$$

Euler's predictor step allows the first approximation of eigenpairs for the new frequency by Eq. (29).

In order to guarantee conversion, *corrector steps* following the predictor step need to be performed. Linear increments for the $i+1$th corrector step of the solution in terms of $\hat{\mathbf{e}}$ and λ, i.e. $\hat{\mathbf{e}}^{i+1} = \hat{\mathbf{e}}^i + \Delta\hat{\mathbf{e}}$, $\lambda^{i+1} = \lambda^i + \Delta\lambda$ are used to set up the static iteration scheme

$$\begin{bmatrix} \mathbf{T} - \lambda^i\mathbf{I} & -\hat{\mathbf{e}}^i \\ -2\hat{\mathbf{e}}^{i^{\mathrm{H}}} & 0 \end{bmatrix}\begin{bmatrix} \Delta\hat{\mathbf{e}} \\ \Delta\lambda \end{bmatrix} = \begin{bmatrix} -(\mathbf{T} - \lambda^i\mathbf{I})\hat{\mathbf{e}}^i \\ 1 - \hat{\mathbf{e}}^{i^{\mathrm{H}}}\hat{\mathbf{e}}^i \end{bmatrix}. \tag{34}$$

The normalization condition $\hat{\mathbf{e}}^{i+1^{\mathrm{H}}}\hat{\mathbf{e}}^{i+1} = 1$ is applied. The correction according to Eq. (34) is repeated until the residuum $r = \|(\mathbf{T} - \lambda^i\mathbf{I})\hat{\mathbf{e}}^i\|_2 < \varepsilon$, where ε is a user-specified limit to quantify the accuracy of the numerical solutions. The eigenpath analysis includes the capacity of automatically tracking crossings or repelling branches in the dispersion diagram, since an evolution of the wave mode shapes is performed over frequency rather than a pure tracking of the eigenvalues representing wavenumbers.

The efficiency of the eigenpath analysis compared to computation of the full eigenvalue problem depends on the number of tracked branches and the resolution of ω_j. If $\Delta\omega$ is chosen very small in order to obtain a fine resolution of the dispersion curves, the predictor step can be omitted, since the solution stays in the close vicinity for the following ω_{j+1}. In addition, the number of static iterations in the corrector step decreases as a result. In the dispersion diagram in Fig. 3 for 150 discrete frequencies, tracking of five curves approximately needs as much computing time as the repeated use of a full eigensolver. Larger model sizes with more DOFs may result in an even better performance of the eigenpath analysis. It is worth noticing that the eigenpath analysis accelerates solutions, if one is only interested in particular branches, for example for parameter variations.

6. Conclusion

The practical advantages of the proposed methodology based on solutions of eigenvalue problems are manifold. First, any pipes with geometries being homogeneous in longitudinal direction can be considered, if FE-models are available. This includes thick-wall cylinders, anisotropic materials, linear damping models, multiple layers or non-annular cross sections. Considering the fact that modern commercial FE packages offer a tremendous variety of element types, a large class of fluid filled pipe problems may be considered, which cannot be solved easily by means of analytical approaches. It is also worth noticing that analytical models require special numerical solvers to find roots of the corresponding transcendental eigenvalue problem [21,22]. Even though the dimension of dispersion equations for fluid filled pipes is of small size, they require large computing times due to the choice of proper initial values and due to the iterative solution of strongly nonlinear equations. Furthermore, analytical models are not available for a large class of problems. These drawbacks are clearly circumvented by the presented WFE-method. Furthermore, the development of special waveguide finite elements is not needed, such that engineers and scientists can employ standard tools for this analysis. The most important advantage is the simple practical use of this postprocessing tool, which may be applied as a black-box tool, transferring a standard linear FE model with arbitrary cross-sectional complexity to a complete dispersion diagram.

Future applications may include the analysis of the harmonic wave motion in ripple pipes, which have non-uniform but periodic properties. The presented method needs to be complemented by dynamic condensation [11]. Furthermore, transfer matrices representing segment models might be continued periodically in order to obtain dynamic models for larger piping segments, which could be combined with standard structural models at interfaces [23] allowing structural analysis of complex pipe assemblies. This can be considered as model reduction on a wave-mode basis, which might reduce memory needs and may extend harmonic analysis to higher frequencies compared to standard FE analysis.

Acknowledgements

Funding of this project by the German Research Society DFG in the Transfer Unit TFB 51 ''Simulation and Active Control of Hydroacoustics in Flexible Piping Systems'' is gratefully acknowledged.

References

[1] P. Kohmann, *Ein Beitrag zur Lärmminderung bei flüssigkeitsbefüllten Rohrleitungen auf Schiffen*, Bericht aus dem Institut A für Mechanik, Stuttgart, 1995.

[2] C.A.F. de Jong, *Analysis of Pulsations and Vibrations in Fluid-Filled Pipe Systems*, TNO Institute of Applied Physics, Delft, Eindhoven, 1998.

[3] Y. Gao, M.J. Brennan, P.F. Joseph, J.M. Muggleton, O. Hunaidi, A model of the correlation function of leak noise in elastic buried pipes, *Journal of Sound and Vibration* 277 (2004) 133–148.

[4] H. Lamb, On the velocity of sound, as affected by the elasticity of the wall, *Manchester Memoirs* 17 (9) (1898) 1–16.

[5] Y.P. Guo, Approximate solutions of the dispersion equation for fluid-loaded cylindrical shells, *Journal of the Acoustical Society of America* 95 (3) (1994) 1435–1445.

[6] W. Kuhl, Die Eigenschaften wassergefüllter Rohre für Widerstands- und Schallgeschwindigkeitsmessungen, *Acustica* 3 (1953) 111–123.

[7] G. Pavic, Acoustical analysis of pipes with flow using invariant field functions, *Journal of Sound and Vibration* 263 (2003) 153–174.
[8] C.R. Fuller, F.J. Fahy, Characteristics of wave propagation and energy distributions in cylindrical elastic shells filled with fluid, *Journal of Sound and Vibration* 81 (4) (1982).
[9] S. Finnveden, C.-M. Nilsson, Waveguide finite elements for fluid-shell coupling, *Eleventh International Congress on Sound and Vibration*, Stockholm, 2003, pp. 501–518.
[10] B.R. Mace, D. Duhamel, M.J. Brennan, L. Hinke, Wave number prediction using finite element analysis, *Eleventh International Congress on Sound and Vibration*, St. Petersburg, 2004, pp. 3241–3248.
[11] B.R. Mace, D. Duhamel, M.J. Brennan, L. Hinke, Wave number prediction using finite element analysis, *Journal of the Acoustical Society of America* 117 (2005) 2835–3843.
[12] F. Fahy, *Structural Sound and Vibration*, Academic Press, London, 1998.
[13] O.C. Zienkiewicz, R.L. Taylor, *The Finite Element Method*, *Vol. I*, Butterworth-Heinemann, 2000.
[14] M. Maess, L. Gaul, Dispersion in fluid-filled pipes by analyzing finite element models, *Proceedings of 31 Deutsche Jahrestagung für Akustik DAGA*, München, 2005.
[15] M. Maess, L. Gaul, Substructuring and model reduction of pipe components interacting with acoustic fluids, *Mechanical Systems and Signal Processing*, 2005, accepted for publication.
[16] A. Quarteroni, R. Sacco, F. Saleri, *Numerical Mathematics*, Springer, New York, 2000.
[17] J.D. Achenbach, *Wave Propagation in Elastic Solids*, Elsevier, North-Holland, Amsterdam, 1984.
[18] L. Cremer, M. Möser, *Technische Akustik*, Springer, Berlin, 2003.
[19] H.J.-P. Morand, R. Ohayon, *Fluid–Structure Interaction*, Wiley, New York, 1995.
[20] N. Wagner, L. Gaul, Eigenpath analysis of friction induced vibrations depending on the friction coefficient, *PAMM* 3 (2003) 130–131.
[21] K.V. Singh, Y.M. Ram, Transcendental eigenvalue problem and its applications, *AIAA Journal* 40 (7) (2002) 1402–1407.
[22] N. Wagner, L. Gaul, Eigenpath analysis of transcendental two-parameter eigenvalue problems, in: P. Neittanmäki, T. Rossi, S. Korotov, E. Onate, J. Périaux, D. Knörzer (Eds.), *European Congress on Computational Methods in Applied Sciences and Engineering ECCOMAS*, Jyväskylä, 2004, pp. 501–518.
[23] J.-M. Mencik, M.N. Ichchou, Multi-mode propagation and diffusion in structures through finite elements, *European Journal of Mechanics A/Solids* 24 (2005) 877–898.